Comparative Study of Weak Interactions in Molecular Crystals: H−H Bonds vs Hydrogen Bonds†

David J. Wolstenholme* and T. Stanley Cameron

Department of Chemistry, Dalhousie University, Halifax, N.S., Canada, B3H 4J3

Received: February 24, 2006; In Final Form: May 4, 2006

The crystal structures of tetraphenylphosphonium squarate, bianthrone, and bis(benzophenone)azine are shown to contain a variety of $C-H^{\delta+}\cdots^{\delta+}H-C$ interactions, as well as a variety of C−H···O and $C-H\cdots C_{\pi}$ interactions. Each of these molecules possesses interactions that can possibly be characterized as either H−H bonds or weak hydrogen bonds based on the first four criteria proposed by Koch and Popelier. These interactions have been completely characterized topologically after the multipole refinement of the structures. It appears that weak interactions of the form $C-H^{\delta+}\cdots^{\delta+}H-C$ possess certain correlations between the various properties of the electron density at the bond critical points. The coexistence of the three types of interactions makes it possible to establish similarities and differences in the correlations of these weak interactions. This all leads to a better understanding of H−H interactions and how they fit into the hierarchy of weak interactions.

Introduction

Until recently, hydrogen bonds were generally understood as an electrostatic interaction in which a negatively charged heteroatom *X* is covalently bonded to a positively charged hydrogen atom which in turn attracts another negatively charged heteroatom *Y*.[1] We can therefore denote a hydrogen bond as $X^{\delta-}-H^{\delta+}\cdots Y^{\delta-}$, where the X−H group is known as the hydrogen donor and the Y atom is considered the hydrogen acceptor. The field of hydrogen bonding was further enlarged with the discovery of the dihydrogen bond.[1,2−7] It was found that unusually short H···H contacts (1.7−2.2 Å) existed in X-ray crystallographic structures of organometallic compounds. The dihydrogen bonds were of the form $X^{\delta-}-H^{\delta+}\cdots H^{\delta-}-M^{\delta+}$, where M represented a transition metal.

Evidence has also suggested that closed-shell stabilizing interactions can occur between two hydrogen atoms of similar charge.[1,8] The similarities between the two charges is a result of molecular symmetry or electronic environment of the compound. For instance, in the solid state structures of many organic molecules, two hydrogen atoms of similar charges can come into close contact with each other. Whether this is a result of the crystal packing of the molecule forcing these hydrogen atoms to come into close contact or whether these atoms can form a bonding interaction of their own free will, is still uncertain. However, the presence of a bond path between the two hydrogen atoms suggests that a weak bond is formed between the two atoms. Early studies performed by Cioslowski and Mixon on these types of interactions used the classical nonbonding steric interaction theory to describe these interactions as repulsive in nature.[9] However, experimental and theoretical studies of $C-H^{\delta+}\cdots H^{\delta+}-C$ interactions based on isotropic interaction potentials of intermolecular (CH_4) molecules has shown that these interactions possess bond energies on the order of 0.4 kcal/mol.[10,11] Thus, on the basis of energetic considerations obtained from both experimental and theoretical studies, it is clear that these systems with C−H···H−C interactions (in which there is no net electrical charges on the hydrogen atoms or very small charges of the same sign) can exhibit energetic stability, potentials typical of a bound system and stable equilibrium geometry. Therefore, these interactions are quite different from other types of interactions such as dihydrogen bonds and are best classified as H−H bonds.

The aim of this work is to determine if these H−H bonds can be specifically distinguished from a general population of weak hydrogen interactions. This will be attempted using experimental charge density studies, the related topological studies within the context of the theory of "atoms in molecules" (AIM).

The theory of AIM has been applied both experimentally and theoretically to a wide variety of structures containing different types of hydrogen interactions, ranging from hydrogen bonds to van der Waals interactions. This theory states that in a bound molecular state, the nuclei of the bonded atoms are linked by a line in which the electron density is a maximum with respect to any neighboring lines, and is referred to as a bond path (BP).[8] The minimum in the electron density along the bond path is called the bond critical point (BCP), and can be considered as a gateway between two bonded atoms. The BCP possesses several important features such as the electron density at the BCP (ρ_{cp}) and the Laplacian ($\nabla^2\rho_{cp}$), which can be used to characterize the type of bonding that is occurring between the atoms of interest. In the case of an open-shell interaction (covalent bonds) $\rho_{cp} > 0.5$ e Å^{-3}, where in a closed-shell interaction (hydrogen bond or van der Waals interactions) values of ρ_{cp} are generally lower than 0.5 e Å^{-3}. The $\nabla^2\rho(r)$ can be defined as the sum of the eigenvalues of the Hessian matrix ($\nabla^2\rho(r) = \lambda_1 + \lambda_2 + \lambda_3$), the first two curvatures (λ_1, λ_2) are negative and are perpendicular to the bond path, and the third curvature is positive and is tangential to the bond path.[1] When the $\nabla^2\rho(r) < 0$, the density is locally concentrated, resulting in a open-shell interaction, and when $\nabla^2\rho(r) > 0$, the density is

* Corresponding author. Telephone number: 1-(902)-494-3759. Fax number: 1-(902)-494-1310. E-mail: dwolsten@dal.ca.

† CCDC 299197 and 299198 contain the supplementary crystallographic data for this paper. These data can be obtained free of charge via www.ccdc.cam.ac.uk/data_request/cif, or by e-mailing data_request@ccdc.cam.ac.uk, or by contacting The Cambridge Crystallographic Data Centre, 12 Union Road, CB2 1EZ, U.K.; fax +44 1223 336033.

10.1021/jp061205i CCC: $33.50
Published on Web 06/20/2006

locally depleted such as a closed shell interaction. The energy densities at the BCP are another useful way of classifying the type of chemical bonding occurring in a desired system. It has been well established that the kinetic energy density, $G(r_{cp})$, and the potential energy density, $V(r_{cp})$, for a closed-shell interactions can be determined from the following two equations:[12]

$$G(r_{cp}) = (3/10)(3\pi^2)^{2/3}\rho^{5/3}(r_{cp}) + (1/6)\nabla^2\rho(r_{cp}) \quad (1)$$

$$V(r_{cp}) = (\bar{h}^2/4m)\nabla^2\rho(r_{cp}) - 2G(r_{cp}) \quad (2)$$

This means that closed-shell interactions will be dominated by a local excess in the kinetic energy and open-shell interactions will be dominated by a lowering of the potential energy.[1,13] The total energy density can then be calculated from the sum of the local and potential energy densities, as in

$$E(r_{cp}) = G(r_{cp}) + V(r_{cp}) \quad (3)$$

It is important to be able to characterize the type of bonding occurring in weak intra/intermolecular interactions because these weak interactions have been shown to play an important role in the stability of molecular crystals.[14] One group of weak interactions that has received considerable attention over the years is hydrogen bonds, in particular dihydrogen bonds. Recently, it was proposed that dihydrogen bonds of the form $X-H^{\delta+}\cdots{}^{\delta+}H-Y$ should be classified separately from traditional dihydrogen bonds ($X-H^{\delta+}\cdots{}^{\delta-}H-Y$) as a consequence of their differences in atomic and geometric characteristics.[8] The nature of the atoms involved in what is now called H−H bonding is quite difference from that of dihydrogen bonds. H−H bonds generally possess two electronegative atoms covalently bonded to the two hydrogen atoms. Dihydrogen bonds involve both an electronegative and an electropositive atom covalently bonded to their respective hydrogen atoms. The second major difference between the two types of interactions involves the X−H bond lengths. In H−H bonds, the X−H bond length decreases upon formation of the bond, whereas in dihydrogen bonds the X−H bond length increases upon formation of the bond. The atomic volumes of the hydrogen atoms in H−H bonds decrease upon the formation of a bond but to a lesser extent than in the dihydrogen bond. In most cases the decreases in atomic volume for each hydrogen atom in H−H bonds are identical or very similar. The atomic energies of the hydrogen atoms for both interactions are also quite different. Both hydrogen atoms in H−H bonds are stabilized by typically 2−7 kcal/mol, whereas the acidic hydrogen in dihydrogen bonds experiences a marked destabilization of up to 20−40 kcal/mol.[1] Finally, the most obvious difference between the two types of weak interactions is the charges associated with each hydrogen atom. The hydrogen atoms for H−H bonds are both positively charged, whereas dihydrogen bonds have one hydrogen with a positive charge and one hydrogen with a negative charge.

The present paper considers 50 weak intra/intermolecular interactions ranging from C−H···O hydrogen bonds to H−H bonds for three molecular crystals (Figure 1). From these 50 interactions a series of correlation can be obtained using several properties of the electron density at the BCP. These correlations allow the H−H bonds to be clearly distinguished from other types of weak interactions such as hydrogen bonds.

Experimental Section

Three colorless prism crystals (tetraphenylphosphonium squarate, bianthrone, and bis(benzophenone)azine) were mounted on the end of Lindmann glass capillaries, because a tube has a greater resistance to vibration than a fiber of the same cross section. The high-resolution single-crystal X-ray diffraction data were collected on a Rigaku Saturn CCD diffractometer using Mo Kα radiation. The crystal data from the X-ray diffraction experiments can be found in Table 1. The tetraphenylphosphonium squarate (TPS)[15] set of data was collected at a temperature of -180 ± 1 °C to a maximum 2θ value of 90.9°, the bianthrone (BIAN) and bis(benzophenone)azine (AZINE) sets of data were collected at a temperature of -160 ± 1 °C to maximum 2θ values of 82.9° and 82.2°, respectively. The TPS data were collected with 8 scans, each containing 36 images with an exposure time of 36 s/°, and slices of ω between 20 and 200 in increments of 5° ($\chi = 0°$, 45°, and $\phi = 0°$, 90°, 180°, 270°). A total of 720 oscillation images were collected for the BIAN compound, in which a series of data sweeps were performed using ω scans from −47.0 to +133.0° in increments of 1.0° ($\chi = 0°$ and $\phi = 0°$, $\chi = 45°$ and $\phi = 0°$, $\chi = 45°$ and $\phi = 90°$,

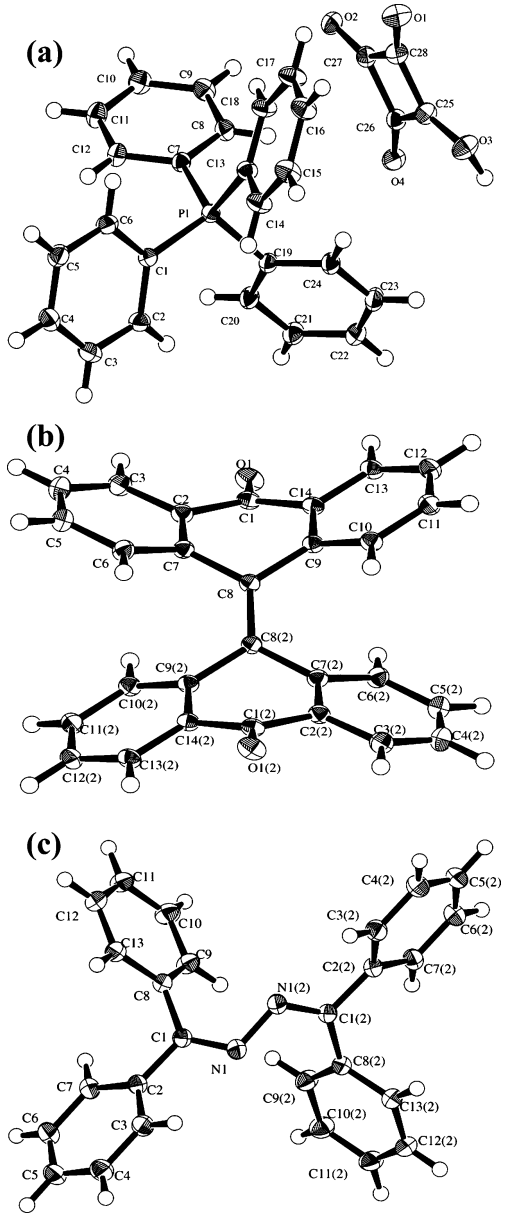

Figure 1. (a) ORTEP diagram with labels for atoms of tetraphenylphosphonium squarate at 90 K with 50% ellipsoid probability. (b) ORTEP diagram with labels for atoms of bianthrone at 90 K with 50% ellipsoid probability. (c) ORTEP diagram with labels for atoms of bis(benzophenone)azine at 90 K with 50% ellipsoid probability.

TABLE 1: Experimental X-ray Data

compound formula	tetraphenylphosphonium squarate $C_{28}H_{21}O_4P$	bianthrone $C_{14}H_8O$	bis(benzophenone)azine $C_{13}H_{10}N$
crystal sizes	0.2 × 0.2 × 0.2	0.24 × 0.2 × 0.18	0.2 × 0.2 × 0.22
formula weight	452.45	192.22	180.23
space group	*P*21/*n* (No. 14)	*P*21/*n* (No. 14)	*C*2/*c* (No. 15)
temperature (°C)	−180	−160	−160
a (Å)	13.2849(3)	10.155(9)	21.909(7)
b (Å)	12.1411(2)	8.327(7)	5.415(2)
c (Å)	14.6423(3)	11.656(11)	16.063(5)
α (deg)	90.0	90.0	90.0
β (deg)	109.7180(12)	109.47(3)	94.427(4)
γ (deg)	90.0	90.0	90.0
V (Å^3)	2223.23(8)	929.3(14)	1899.9(10)
Z	4	4	8
D_c (g/cm)	1.352	1.374	1.260
F(000)	944.00	400.00	760.00
μ (mm^{-1})	1.57	0.85	0.74
radiation	Mo Kα	Mo Kα	Mo Kα
reflection no. (unique)	12107	5943	5628
R(*F*)	1.94%	4.75%	5.72%
$R_w(F)$	1.92%	2.14%	3.72%
GOF	2.1484	2.2058	2.6053
collection range	$-26 \le h \le 26$; $-23 \le k \le 24$; $-29 \le l \le 29$	$-18 \le h \le 18$; $-15 \le k \le 14$; $-20 \le l \le 16$	$-39 \le h \le 36$; $-6 \le k \le 9$; $-29 \le l \le 29$
maximum resolution (2*θ*)	90.9	82.9	82.2

$\chi = 45°$ and $\phi = 180°$). A total of 2160 oscillation images were collected for the AZINE compound, in which 8 scans were performed, with half the scans having an exposure time of 40 s/° and the other half having an exposure time of 80 s/°. These scans were taken with slices of ω between −48.0 to 72.0° in increments of 0.5° ($\chi = 0°$ and $\phi = 0°$, $\chi = 45°$ and $\phi = 0°$, $\chi = 45°$ and $\phi = 90°$, $\chi = 45°$ and $\phi = 180°$) for both exposure times. The crystal-to-detector distances were 127.0, 39.78, and 39.58 mm, respectively. This strategy provided high resolution, large redundancy, and better completeness in the data sets, which are key factors for multipole refinement modeling. The data collection was monitored and reduced with *hkl*2000[16] (TPS) and CrystalClear[17] (BIAN, AZINE) packages, and sorting, scaling, and merging of the intensities were performed with Sortav[18] as included in the WinGX[19] software. All three structures were solved by direct methods and expanded using Fourier techniques through the CrystalStructure software package.[20] All of the molecular thermal ellipsoid plots were generated using the ORTEP-3 program.[21] The CIF file was deposited in the Cambridge Crystallographic Data Centre.

Multipole Refinement

The experimental measurements and analysis of the charge densities of the three compounds have been achieved through the use of high-resolution X-ray diffraction data at low temperatures. The charge density of each compound was then evaluated through the interpretation of its electron density. The method of multipole expansion used to obtain the electron density was through the multipole expansion, which incorporates the Hansen−Coppens model[22] and can be expressed by the following equation:

$$\rho(r) = P_c\rho_{core}(r) + P_v\kappa^3\rho_{valence}(\kappa r) + \sum_{l_{max}}^{l_0}\kappa'^3 R_l(\kappa' r)\sum_{m=0}^{l} P_{lm\pm} d_{lm\pm}(\theta,\varphi) \quad (4)$$

where ρ_{core} and $\rho_{valence}$ are spherically averaged Hartree−Fock core and valence densities, $d_{lm\pm}$ represents the spherical harmonic angular functions, R_l is the radial function, κ and κ' are the expansion−contraction parameters, and P_v and $P_{lm\pm}$ represent the population parameters.

The multipole refinements were carried out with the module XDLSM incorporated in the software package XD.[23] The residual bonding density not modeled in the conventional spherical refinements, was taken into account in the multipole refinements.[24] The scattering factors used in the multipole refinements were those derived by Clementi and Roetti for all atoms.[25] The least-squares refinements involved the minimization of the $\sum w(|F_0|^2 - K|F_c|^2)^2$ function for all reflections with $I > 3\sigma(I)$. The multipole expansion was then applied up to the octapole level ($l_{max} = 3$) for all of the carbon, oxygen, nitrogen atoms except phosphorus, which was expanded up to the hexadecapole level ($l_{max} = 4$). The multipole expansion for the hydrogen atoms was applied up to the dipole level ($l_{max} = 1$). Initially, the κ and κ' parameters were employed for heavy atoms that were chemically different until a reasonable model was achieved. The expansion/contraction parameters of the hydrogen atoms were left fixed at the default XDLSM value of 1.2. To determine accurate positional and thermal parameters for the heavy atoms, a high-order ($\sin\theta/\lambda \ge 0.6$ or 0.7 Å) refinement was performed for each structure. Low-order ($\sin\theta/\lambda \le 0.6$ or 0.7 Å) refinements were then performed to obtain initial positional and accurate isotropic thermal parameters for all the hydrogen atoms. Due to the unavailability of the neutron data, the positions of the H-atoms throughout these refinements were fixed to average bond distance values obtained from reported neutron diffraction studies of similar compounds ($C_{ar}-H = 1.08$ Å).[26,27] The charge neutrality constraint was applied throughout the multipole refinements of all three compounds to achieve an overall neutral molecule. A general multipole refinement strategy was then applied to all three compounds as follows: (a) scale factor, (b) P_v for all heavy atoms, (c) P_v for all hydrogen atoms, (d) κ for all heavy atoms, (e) P_{lm} for all heavy atoms, (f) P_{lm} for all hydrogen atoms, (g) κ for all heavy atoms, (h) P_vP_{lm} for all atoms, (i) κ' for all heavy atoms, (j) positional and thermal parameters for all heavy atom, and finally (k) everything together except κ'. This procedure was then cycled through until

TABLE 2: Intermolecular Properties of the H−H Bond Critical Points

molecule	interaction	$\rho(r_{cp})$, e Å^{-3}	$\nabla^2\rho(r_{cp})$, e Å^{-5}	R_{ij}, Å	λ_1, e Å^{-5}	λ_2, e Å^{-5}	λ_3, e Å^{-5}
TPS	H(3)···X2_H(21)	0.047	0.724	2.17	−0.20	−0.15	1.08
TPS	H(18)···X2^1_H(5)	0.035	0.53	2.35	−0.12	−0.1	0.75
TPS	H(12)···X3_H(12)	0.013	0.166	3.07	−0.03	−0.01	0.2
BIAN	H(3)···X3^1_H(3)	0.018	0.306	2.57	−0.05	−0.04	0.39
BIAN	H(3)···X3^1_H(4)	0.012	0.237	2.71	−0.03	0.00	0.27
BIAN	H(5)···X3^2_H(5)	0.006	0.08	3.28	−0.01	−0.01	0.1
BIAN	H(6)···X4_H(12)	0.022	0.494	2.28	−0.07	−0.07	0.63
AZINE	H(3)···X6_H(12)	0.016	0.285	2.67	−0.05	−0.02	0.35
AZINE	H(4)···X6_H(12)	0.016	0.322	2.58	−0.06	−0.03	0.41
AZINE	H(6)···X4_H(13)	0.016	0.349	2.44	−0.06	−0.05	0.45
AZINE	H(9)···X2^2_H(9)[a]	0.078	1.127	1.91	−0.34	−0.33	1.80
AZINE	H(10)···X5_H(10)	0.034	0.671	2.18	−0.16	−0.10	0.93

molecule	interaction	$G(r_{cp})$, kJ/(mol bohr^3)	$V(r_{cp})$, kJ/(mol bohr^3)	$E(r_{cp})$, kJ/(mol bohr^3)	$\Delta r_H + \Delta r_B$, Å	$\Delta r_H - \Delta r_B$, Å	bond energy, kJ/(mol bohr^3)
TPS	H(3)···X2_H(21)	15.06	−10.40	4.66	0.229	0.101	−5.20
TPS	H(18)···X2^1_H(5)	10.80	−7.16	3.64	0.050	0.136	−3.58
TPS	H(12)···X3_H(12)	3.24	−1.96	1.28	−0.673	0.000	−0.98
BIAN	H(3)···X3^1_H(3)	5.94	−3.55	2.39	−0.166	0.000	−1.78
BIAN	H(3)···X3^1_H(4)	4.50	−2.55	1.96	−0.306	0.200	−1.27
BIAN	H(5)···X3^2_H(5)	1.52	−0.85	0.66	−0.875	0.000	−0.43
BIAN	H(6)···X4_H(12)	9.51	−5.57	3.94	0.119	0.187	−2.78
AZINE	H(3)···X6_H(12)	5.49	−3.22	2.27	−0.271	−0.177	−1.61
AZINE	H(4)···X6_H(12)	6.16	−3.56	2.61	−0.179	−0.186	−1.78
AZINE	H(6)···X4_H(13)	6.65	−3.80	2.85	−0.042	−0.017	−1.90
AZINE	H(9)···X2^2_H(9)[a]	24.92	−19.14	5.78	0.487	0.000	−9.57
AZINE	H(10)···X5_H(10)	13.30	−8.32	4.98	0.219	0.000	−4.16

	symmetry			
interaction	*xyz*	TA	TB	TC
X2	$^1/_2 - X$, $^1/_2 + Y$, $^1/_2 - Z$	0	−1	1
X2^1	$^1/_2 - X$, $^1/_2 + Y$, $^1/_2 - Z$	0	−1	0
X2^2	$-X$, $+Y$, $^1/_2 - Z$	1	0	0
X3	$-X$, $-Y$, $-Z$	1	0	1
X3^1	$-X$, $-Y$, $-Z$	1	1	0
X3^2	$-X$, $-Y$, $-Z$	1	1	1
X4	$^1/_2 - X$, $^1/_2 + Y$, $^1/_2 - Z$	0	0	0
X5	$-X$, $+Y$, $^1/_2 - Z$	1	0	0
X6	$+X$, $-Y$, $^1/_2 + Z$	0	0	−1

[a] C−H$^{\delta+}$···$^{\delta+}$H−C intramolecular interactions.

convergence was achieved. The XDPROP program incorporated into the XD[23] package was then used to determine the total electron density et the BCP $\rho(r_{cp})$, the Laplacian, and the ellipticity for all the intra/intermolecular interactions for the three compounds of interest. All static, residual, dynamic, and deformation maps were produced using the XDGRAPH option in the XD[23] package.

Results and Discussion

Unlike many of the crystal structures containing dihydrogen bonds or H−H bonds reported in the literature, the structures of TPS, BIAN, and AZINE possess at least two distinct intra/intermolecular H−H interactions shorter then 3.2 Å, along with a variety of other weak interactions.[28] An advantage of this is that the H−H interactions can be directly compared with corresponding hydrogen bonds in term of the properties of the electron density at the BCP. The majority of the H−H interactions reported in the literature are based on geometrical evidence for bonding.[28] Here, the interactions observed in these compounds were completely characterized on the basis of their topology. This offers a better understanding of the bonding occurring in these molecules than geometrical evidence alone. For H−H interactions to be characterized as either dihydrogen bonds or H−H bonds, a set of criteria must be satisfied. According to Popelier, dihydrogen bonds can be characterized using the same criteria proposed for hydrogen bonds.[2,29] Thus, the first four Popelier topological criteria will be applied here to all the intra/intermolecular H−H interactions for the three title compounds.

The 50 interactions found in TPS,[15] BIAN, and AZINE can be separated into three types of interactions, C−H···C_π, C−H···O, or C−H$^{\delta+}$···$^{\delta+}$H−C. There are 21 C−H···C_π intermolecular interactions (9 from TPS,[15] 7 from BIAN, and 5 from AZINE). Also, the TPS and BIAN structures possess 16 C−H···O interactions (13 from TPS[15] and 3 from BIAN). All 13 of the C−H···O interactions from TPS[15] are intermolecular interactions, whereas two of the BIAN interactions are intermolecular and one is intramolecular. There are also 12 interactions between the three compounds that have the form C−H$^{\delta+}$···$^{\delta+}$H−C (3 from TPS,[15] 4 from BIAN, and 5 from AZINE). All of the C−H$^{\delta+}$···$^{\delta+}$H−C contacts in the three compounds except one are intermolecular interactions. The one intramolecular C−H$^{\delta+}$···$^{\delta+}$H−C interaction exists in the AZINE molecule and represents the shortest bond path length (1.91 Å) for all of the molecules used in this study. It should be noted that 7 of the C−H···O interactions (5 from TPS[15] and 2 from BIAN) can be classified as hydrogen bonds on the basis of the first four criteria proposed by Popelier. Only 2 of the C−H···C_π interactions can be classified as hydrogen bonds, both of which are found in the TPS[15] molecule. The rest of the C−H···O and C−H···C_π interactions are best described as weak van der Waals interactions. The details regarding the application of these criteria for both C−H···O and C−H···C_π interactions will not be discussed in this paper.

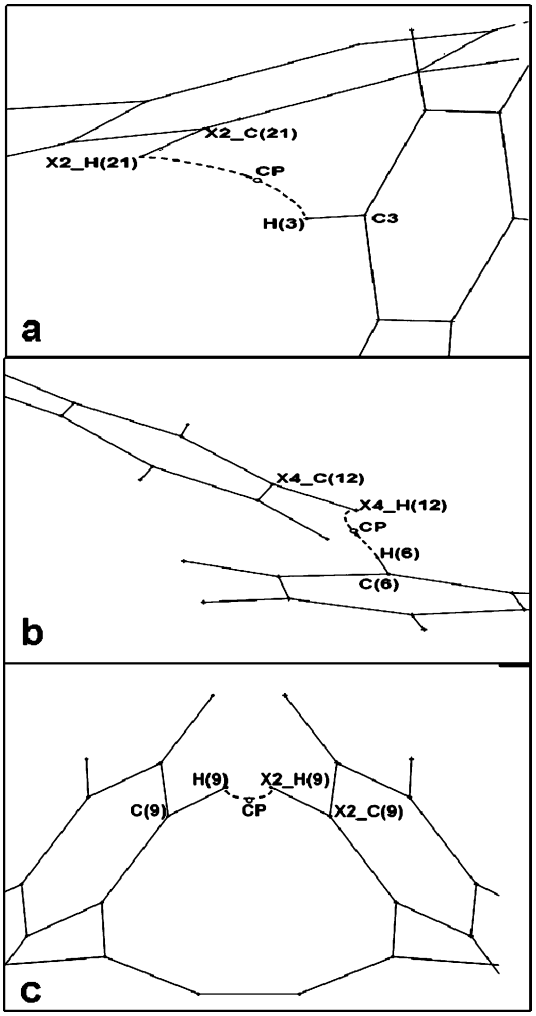

Figure 2. (a) Bond path character in tetraphenylphosphonium squarate showing the critical point locations along the C−H···H−C interactions shown in dashed lines. (b) Bond path character in bianthrone showing the critical point locations along the C−H···H−C interactions shown in dashed lines. (c) Bond path character in bis(benzophenone)azine showing the critical point locations along the C−H···H−C interactions shown in dashed lines

The local properties of all the C−H$^{\delta+}$···$^{\delta+}$H−C interactions observed in the three compounds can be found in Table 2. The *xyz* and translations of the symmetry related molecules used throughout the text can also be found at the end of Table 2. Below we discuss each C−H$^{\delta+}$···$^{\delta+}$H−C interaction in terms of the first four criteria proposed by Koch and Popelier:[29] (a) a rational bond path (BP) with a reasonable critical point (BCP), adequate values of (b) the electron density ($\rho(r_{cp})$), and (c) the Laplacian ($\nabla^2\rho(r_{cp})$) at the BCP and (d) mutual penetration of the donor and acceptor atoms.

The first criterion essentially establishes that a bond could exist once there is a reasonable topology for the bond.[29] Thus for the H−H bond to be considered, the interaction must possess a consistent BP and BCP between its donor and acceptor atoms. All 12 C−H$^{\delta+}$···$^{\delta+}$H−C interactions in the three molecules possess consistent BPs and BCPs, and therefore satisfy this criterion. Examples are shown in Figure 2a−c, where an experimental bond path is traced along one of the C−H$^{\delta+}$···$^{\delta+}$H−C interaction found in each of the three compounds.

The second criterion requires that the $\rho(r_{cp})$ values at the BCP fall within a certain range, typically between 0.013 and 0.27 e Å^{-3} for weak interactions. There must also be a relationship between $\rho(r_{cp})$ and the energy densities for this criterion to be completely satisfied. It is clear from the $\rho(r_{cp})$ values in Table 2 that all the C−H$^{\delta+}$···$^{\delta+}$H−C interactions in TPS[15] and AZINE are within the desired range. Although only three of the four C−H$^{\delta+}$···$^{\delta+}$H−C interactions in BIAN were found to satisfy the $\rho(r_{cp})$ requirement. The C(5)−H(5)$^{\delta+}$···$^{\delta+}$X3^2_H(5)−X3^2_C(5) interaction has a $\rho(r_{cp})$ value of 0.006 e Å^{-3}, which means it is better classified as a weak van der Waals interaction. After criterion two, there are now 11 remaining satisfactory H−H interactions.

However, in addition to the electron density ($\rho(r_{cp})$) restriction in criterion two, $\rho(r_{cp})$ must also correlate with the energy densities. For the H−H interactions these correlations may help to identify the interactions as a separate population. It has previously been shown that the $\rho(r_{cp})$ values in H−H interactions can be correlated with the internuclear distances.[28] In a similar fashion, it can be shown that the $\rho(r_{cp})$ values in all three compounds are exponentially correlated to their interaction lengths for both C−H$^{\delta+}$···$^{\delta+}$H−C and C−H···C$_\pi$/C−H···O interactions (Figure 3). The C−H$^{\delta+}$···$^{\delta+}$H−C correlation shows a fit of 91% and the C−H···C$_\pi$/C−H···O correlation shows a fit of 80%. When comparing the C−H$^{\delta+}$···$^{\delta+}$H−C correlations against the correlations of the other weak interactions, one can

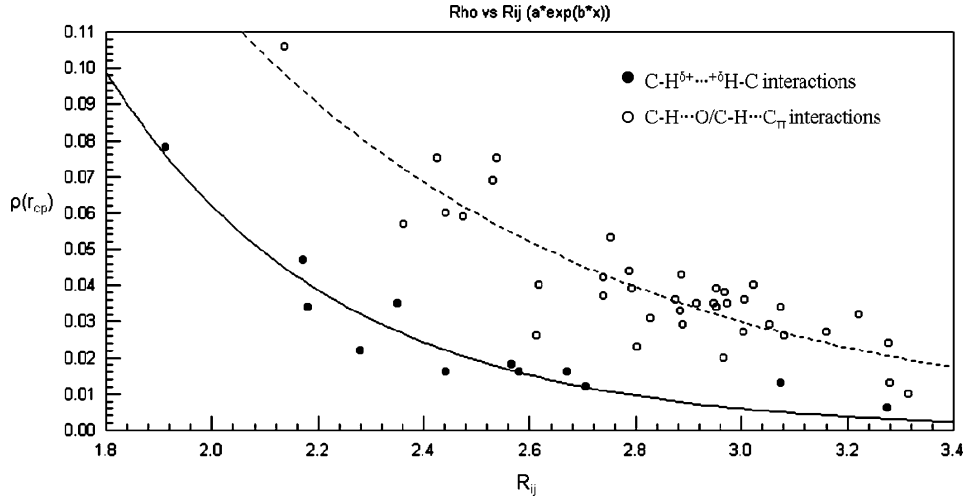

Figure 3. Exponential dependence of ρ_{cp} [e Å^{-3}] on the interaction length, R_{ij} (Å), for all the weak interactions of TPS, BIAN, and AZINE. The dashed line represents the fitting of C−H···C$_\pi$ and C−H···O interactions ($R^2 = 0.80$). The solid line represents the fitting of C−H$^{\delta+}$−$^{\delta+}$H−C interactions ($R^2 = 0.91$).

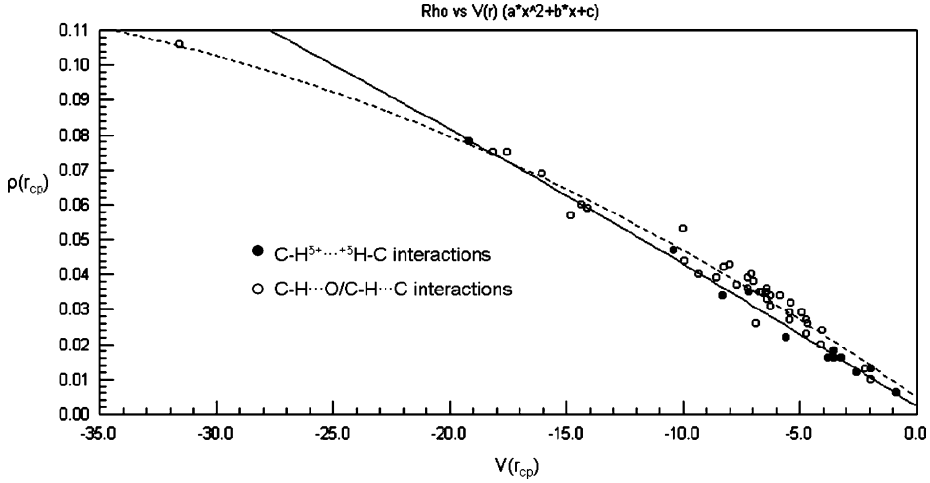

Figure 4. Quadratic dependence of ρ_{cp} (e Å^{-3}) on the potential energy density, $V(r_{cp})$ [kJ/(mol bohr^3)], for all the weak interactions of TPS, BIAN, and AZINE. The dashed line represents the fitting of C−H···C_π and C−H···O interactions ($R^2 = 0.97$). The solid line represents the fitting of C−H$^{\delta+}$−$^{\delta+}$H−C interactions ($R^2 = 0.99$).

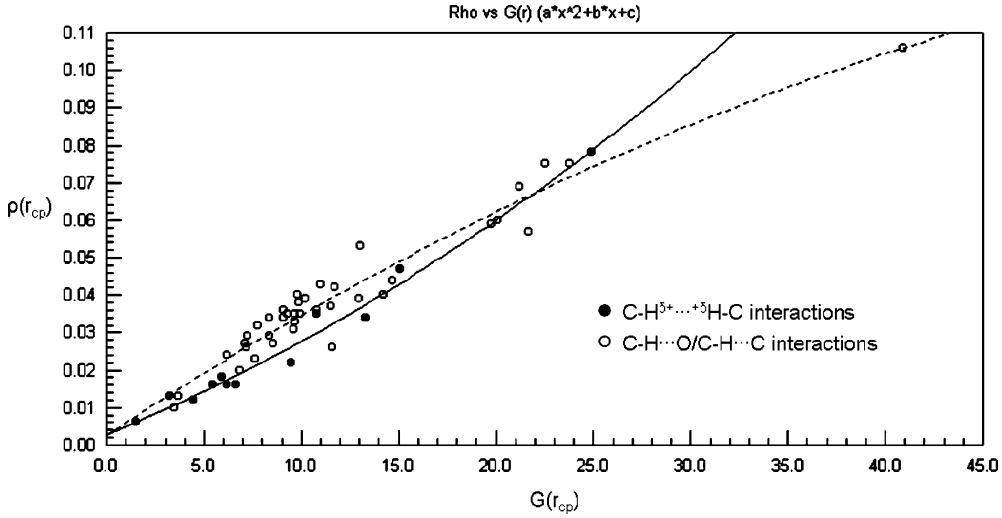

Figure 5. Quadratic dependence of ρ_{cp} (e Å^{-3}) on the kinetic energy density, $G(r_{cp})$ [kJ/(mol bohr^3)], for all the weak interactions of TPS, BIAN, and AZINE. The dashed line represents the fitting of C−H···C_π and C−H···O interactions ($R^2 = 0.94$). The solid line represent the fitting of C−H$^{\delta+}$−$^{\delta+}$H−C interactions ($R^2 = 0.99$).

clearly see that the H−H interactions follow an exponential fitting similar to that of the C−H···C_π/C−H···O interactions. The only major difference between the two exponential fittings is that the H−H correlation is slightly lower along the $\rho(r_{cp})$ axis then the C−H···C_π/C−H···O correlation. Two possible explanations for this difference are as follows: the H−H interactions could have a lower probability of accumulating electron density at the BCP than the other interactions because both the donor and acceptor atoms have only one electron to share between a covalent bond and an intermolecular interaction or the fact that the hydrogen atoms are smaller than all other atoms; therefore, less overlap is likely to occur between two hydrogen atoms compared to other types of interactions.

Another correlation that can be observed for both C−H$^{\delta+}$···$^{\delta+}$H−C and C−H···C_π/C−H···O interactions is between $\rho(r_{cp})$ and the local potential energy density. Figure 4 shows the $\rho(r_{cp})$ values plotted versus the potential energy densities for all three types of weak interactions. The C−H$^{\delta+}$···$^{\delta+}$H−C correlation shows a fit of 99%, and the C−H···C_π/C−H···O correlation shows a fit of 97%. These quadratic fits show that a general increase in $\rho(r_{cp})$ leads to an increase in the potential energy density. It is interesting to note that both types of interactions have almost identical fits, showing that there is little difference in the amount of potential energy density accumulated for either type of interaction.

Figure 5 also shows that the $\rho(r_{cp})$ values are correlated to the kinetic energy densities for all three types of interactions. The C−H$^{\delta+}$···$^{\delta+}$H−C correlation shows a fit of 99%, and the C−H···C_π/C−H···O correlation shows a fit of 94%. Unlike the first correlation, between $\rho(r_{cp})$ and the potential energy densities, these correlations show a slight difference between C−H$^{\delta+}$···$^{\delta+}$H−C and C−H···C_π/C−H···O interactions. The C−H$^{\delta+}$···$^{\delta+}$H−C interactions can be quadratically fit in a concave upward fashion, whereas the C−H···C_π/C−H···O interactions fit the data in a concave downward fashion.

Because a relationship exists between $\rho(r_{cp})$ and the two energy densities, a relationship should also exist between $\rho(r_{cp})$ and the total energy density, $E(r_{cp})$, as this value is determined from the previous two energy densities. Figure 6 shows the exponential dependence of the total energy density on R_{ij}, and it can be seen that it resembles the dependence of $\rho(r_{cp})$ on R_{ij}. The C−H$^{\delta+}$···$^{\delta+}$H−C correlation shows a fit of 96% and the C−H···C_π/C−H···O correlation shows a fit of 95%. This enforces the idea that a relationship must exist between these two parameters. It is clear from the above discussion that the second criterion for hydrogen bonding can

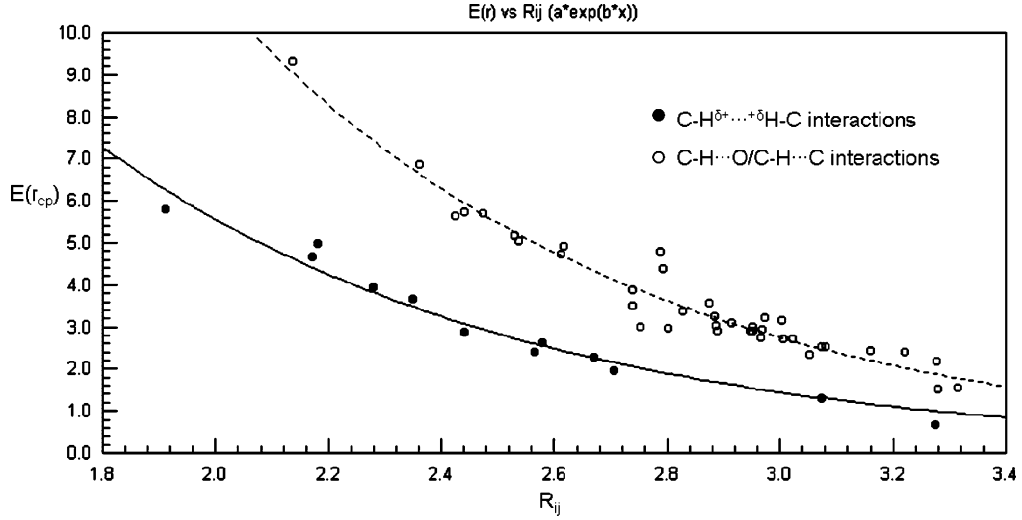

Figure 6. Exponential dependence of $E(r_{cp})$ [kJ/(mol bohr^3)] on the interaction length, R_{ij} (Å), for all the weak interactions of TPS, BIAN, and AZINE. The dashed line represents the fitting of C−H···C_π and C−H···O interactions ($R^2 = 0.95$). The solid line represents the fitting of C−H$^{\delta+}$−$^{\delta+}$H−C interactions ($R^2 = 0.96$).

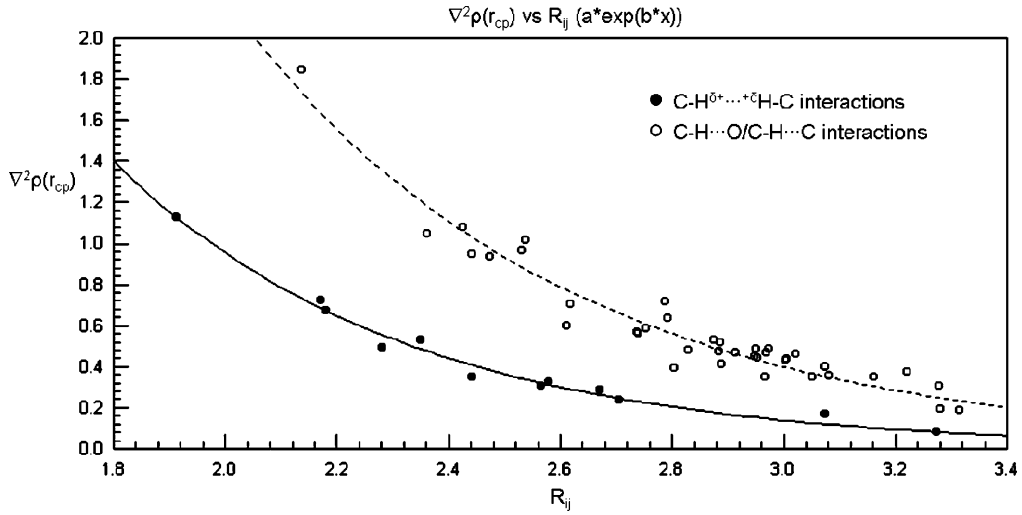

Figure 7. Exponential dependence of $\nabla^2\rho_{cp}$ (e Å^{-5}) on the interaction length, R_{ij} (Å), for all the weak interactions of TPS, BIAN, and AZINE. The dashed line represents the fitting of C−H···C_π and C−H···O interactions ($R^2 = 0.94$). The solid line represents the fitting of C−H$^{\delta+}$−$^{\delta+}$H−C interactions ($R^2 = 0.98$).

also be applied to H−H interactions, and they appear to form separate populations from the C−H···C_π/C−H···O hydrogen bonds.

The third Popelier criterion states that the values of the Laplacian ($\nabla^2\rho_{cp}$) at the BCP must be positive and fall within a certain range, typically between 0.35 and 4.0 e Å^{-5} for weak interactions.[29] Similar to criterion two, $\nabla^2\rho_{cp}$ should also correlate to the energy densities for this criterion to be completely satisfied. Table 2 shows that half the C−H$^{\delta+}$···$^{\delta+}$H−C interactions fall within the required range for H−H bonding (2 from TPS,[15] 1 from BIAN, and 3 from AZINE), this leaves six surviving H−H interactions. The interactions that do not fulfill this criterion are therefore classified as weak van der Waals interactions. A previous study has shown that there exists a correlation between the $\nabla^2\rho_{cp}$ and the internuclear distances for H−H interactions.[28] An exponential dependence exists between $\nabla^2\rho_{cp}$ and R_{ij} for all three types of interactions in this work. The $\nabla^2\rho_{cp}$ values decrease exponentially as the R_{ij} values increase (Figure 7). The C−H$^{\delta+}$···$^{\delta+}$H−C correlation shows a fit of 98% and the C−H···C_π/C−H···O correlation shows a fit of 94%. The only major difference between the two exponential fittings is that the H−H correlation is slightly moved lower along the $\nabla^2\rho_{cp}$ axis than the C−H···C_π/C−H···O correlation. This follows the generally accepted belief that H−H interactions are weaker than C−H···C_π/C−H···O interactions. It should also be noted that the $\nabla^2\rho_{cp}$ values are correlated to the energy densities in a way similar to $\rho(r_{cp})$.

The fourth Popelier criterion involves the mutual penetration of the donor and acceptor atoms. It can be considered essential and sufficient for classifying weak interactions as hydrogen bonds, H−H bonds, or van der Waals interactions. This criterion is measured by looking at the $\Delta r_H + \Delta r_B$ values of each interaction, where Δr_X is simply the nonbonding radius of the acceptor/donor atom minus its bonding radius (see below). The nonbonding radius is taken to be equivalent to the gas-phase van der Waals radius for any particular atom. In this work the nonbonding radius for carbon is taken as 1.85 Å, oxygen as 1.54 Å, and hydrogen as 1.2 Å.[30,31] The bonding radius is simply taken as the distance from the donor/acceptor nucleus to the BCP. For an interaction to be classified as a hydrogen bond/H−H bond, the penetration value ($\Delta r_H + \Delta r_B$) must be positive, which indicates that the van der Waals spheres for the two atoms are overlapping. It is clear from the values in Table 2 that five

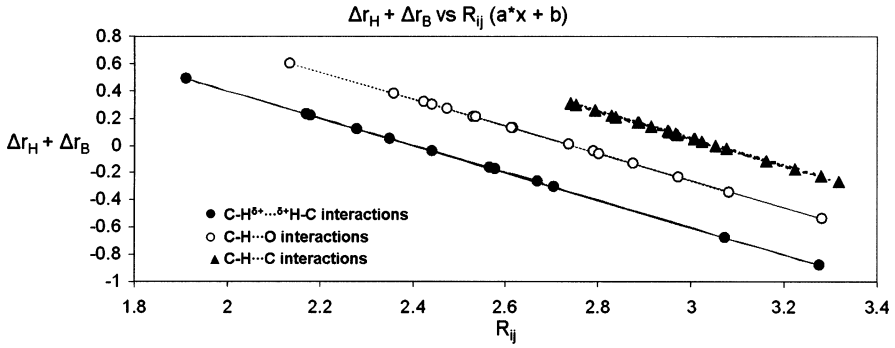

Figure 8. Linear dependence of $\Delta r_H + \Delta r_B$ (Å) on the interaction length, R_{ij} (Å) for all the weak interactions of TPS, BIAN, and AZINE. The dashed lines represent the fitting of C−H···O interactions ($R^2 = 1.0$) and C−H···C interactions ($R^2 = 1.00$). The solid lines represent the fitting of C−H$^{\delta+}$−$^{\delta+}$H−C ($R^2 = 1.00$)

C−H$^{\delta+}$···$^{\delta+}$H−C interactions satisfy the $\Delta r_H + \Delta r_B$ portion of this criterion (two from TPS,[15] one from BIAN, and two from AZINE). Figure 8 shows a linear correlation between each type of weak interaction involving $\Delta r_H + \Delta r_B$ and R_{ij}. Similar correlations for C−H···C_π and C−H···O interactions have previously been reported in the literature,[24,32] but so far, these interaction correlations have not been compared with those for the H−H interactions. Figure 8 clearly shows the separate population for these H−H bonds. All the correlations in Figure 8 show an increase in $\Delta r_H + \Delta r_B$ as the R_{ij} values decrease. This is to be expected because the closer the two atoms are to each other the more the van der Waals spheres should overlap each other, leading to greater penetration. An interesting feature observed between the C−H···C_π correlation and the C−H···O correlation is that the linear fit of the C−H···C_π interactions is moved slightly higher up along the $\Delta r_H + \Delta r_B$ axis than that of the C−H···O interactions. This seems to indicate that the C−H···C_π interactions could lead to a higher degree of mutual penetration than the C−H···O interactions if they possessed smaller R_{ij} values. The C−H$^{\delta+}$···$^{\delta+}$H−C interactions follow a similar linear correlation as the other two types of interactions, except their *y*-intercept is slightly lower along the $\Delta r_H + \Delta r_B$ axis than the C−H···O interactions. This is to be expected, because the C−H$^{\delta+}$···$^{\delta+}$H−C interactions involve two hydrogen atoms that are smaller than any other atom. This leads to less overlap of the van der Waals spheres and less penetration of the donor/acceptor atoms. Another important component of this criterion is the amount in which the BCP penetrates the donor atom's van der Waals sphere in comparison to that of the acceptor atom ($\Delta r_H - \Delta r_B$). Table 2 shows that five of the C−H$^{\delta+}$···$^{\delta+}$H−C interactions satisfy this portion of the criterion (two from TPS,[15] one from BIAN, and two from AZINE). The H(9)···X2^2_H(9) and H(10)···X5_H(10) interactions have $\Delta r_H - \Delta r_B$ values that are equal to zero. Because in each case both hydrogen atoms are chemically equivalent as a result of symmetry. This means they will have the same values for their electron density parameters, including the amount of penetration for each atom. These two interactions can still be considered as H−H bonds because both hydrogen atoms in each interaction are experiencing a significant amount of penetration (0.2437 and 0.1093, respectively). Thus, the fourth criterion can be considered essential for characterizing H−H bonds based on the electron density properties at the BCP.

Further evidence confirming a bonding interaction between these H−H bonds can be seen in there static deformation maps and electrostatic potential maps (Figure 9). The static maps of two hydrogen atoms involved in an H−H bond show a small change in the electron density between the two atoms upon formation of the H−H bonded complex. This is not the case

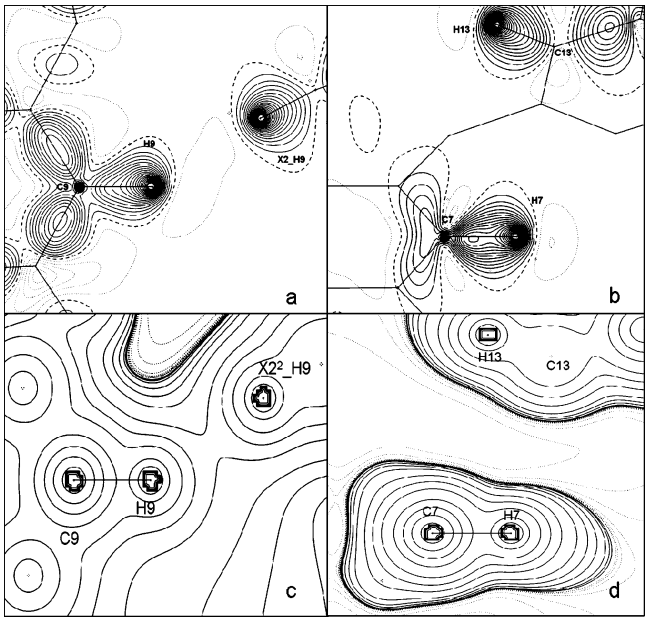

Figure 9. (a) Static map of the intramolecular H−H bond found in the AZINE molecule. (b) Static map between two hydrogen atoms in the AZINE molecule that are not involved in an H−H bond. (c) Electrostatic potential map of the intramolecular H−H bond found in the AZINE molecule. (d) Electrostatic potential map between two hydrogen atoms in the AZINE molecule that are not involved in an H−H bond. The solid lines represent the positive contours, the dotted lines represent the negative contours, and the dashed lines represent the zero contour lines. All contours are taken in increments of 0.05 e Å^{-3}.

for two hydrogen atoms not involved in H−H bonding, where no change in the electron distribution is observed between the two atoms. Because H−H bonds are almost purely electrostatic in nature, it would not be expected to see much difference between the two types of static maps. However, the electrostatic nature of these interactions is clearly shown in the electrostatic potential maps of these interactions. Figure 9c clearly shows that H−H bonds possess some electrostatic potential in the bond confirming a bonding interaction. Although Figure 9d shows that two hydrogen atoms not involved in H−H bond or a weak van der Waals interaction have no electrostatic potential between the two atoms. This seems to justify the idea that two hydrogen atoms of close contact can form a bonding interaction.

Conclusion

Experimental charge density calculations on a series of three organic molecules have lead to the clear characterization of five H−H bonds based on the first four Popelier criteria for hydrogen

bonding. The four intermolecular H−H bonds were found for the interactions H(3)···X2_H(21), H(18)···X2[1]_H(5), H(6)···X4_H(12), and H(10)···X5_H(10) (two tetraphenylphosphonium squarate, one bianthrone, and one bis(benzophenone)-azine, respectively). The only intramolecular H−H bond was found to be the H(9)···X2_H(9) interaction in bis(benzophenone)azine. It has also been shown that the $C-H^{\delta+}\cdots^{\delta+}H-C$ interactions follow many of the same correlations as other weak interactions. These correlations can be used to understand the differences and similarities between $C-H^{\delta+}\cdots^{\delta+}H-C$ interactions and other weak interactions, as well as showing how H−H interactions fit into the hierarchy of weak interactions. Finally, these interactions are of importance because they can play a significant role in determining the conformation of a molecule in its crystalline state as well as its stability.

Acknowledgment. We are indebted to Rigaku/MSC, The Woodlands, TX, for provision of the low-temperature data collection facilities during a Sabbatical Leave Fellowship to T.S.C. We thank the Natural Sciences and Engineering Research Council of Canada for Financial support. We also thank Dr. C. F. Matta and Dr. K. N. Robertson for helpful discussions on the topic.

Supporting Information Available: The final atomic coordinates, anisotropic displacement parameters, bond lengths, multipole population coefficients, κ and κ' values, and deformation maps obtained from the multipole refinement. This material is available free of charge via the Internet at http://pubs.acs.org.

References and Notes

(1) Matta, C. F. In *Hydrogen Bonding-New Insight*; Grabowski, S., Ed.; Challenges and Advances in Computational Chemistry and Physics Series; Kluwer: Amsterdam, 2006.

(2) Crabtree, R. H. *Science* **1998**, *282*, 2000−2001.

(3) Lee Jr., J. C.; Peris, E.; Rheingold, A. L.; Crabtree, R. H. *J. Am. Chem. Soc.* **1994** *116*, 11014−11019.

(4) Richardson, T. B.; de Gala, S.; Crabtree, R. H. *J. Am. Chem. Soc*. **1995**, *117*, 12875−12876.

(5) Crabtree, R. H.; Siegbahn, P. E. M.; Eisenstein, O.; Rheingold, A. L.; Koetzle, T. F. *Acc. Chem. Res*. **1996**, *29*, 348−354.

(6) Klooster, W. T.; Koetzle, T. F.; Siegbahn, P. E. M.; Richardson, T. B.; Crabtree, R. H. *J. Am. Chem. Soc.* **1999**, *121*, 6337−6343.

(7) Crabtree, R. H. *Acc. Chem. Res*. **1990**, *23*, 95−101.

(8) Matta, C. F.; Hernandez-Trujillo, J.; Tang, T. H.; Bader, R. F. W. *Chem. Eur. J.* **2003**, *9*, 1940−1951.

(9) Cioslowski, J.; Mixon, S. T. *Can. J. Chem.* **1992**, *70*, 443−449

(10) Reid, B. P.; O'Loughlin, M. J.; Sparks, R. K. *J. Chem. Phys.* **1985**, *83*, 5656−5662.

(11) Novoa, J. J.; Whangboo, M. H.; Williams, J. M. *J. Chem. Phys*. **1991**, *94*, 4835−4841.

(12) Abramov, Y. A. *Acta Crystallogr*. **1997**, *A53*, 264.

(13) Popelier, P. *Atoms in Molecules. An Introduction*; Prentice Hall: London, 2000.

(14) (a) Desiraju, G. R. *Acc. Chem. Res*. **1991**, *24*, 290−296. (b) Aakeroy, C. B.; Sneddon, K. R. *Chem. Soc. Rev.* **1993**, *22*, 397−407. (c) Desiraju, G. R.; Kashino, S.; Coombs, M. M.; Glusker, J. *Acta Crystallogr*. **1993**, *B49*, 880−892.

(15) Wolstenholme, D. J.; Aquino, M. A.; Cameron, T. S.; Ferrara, J. D.; Robertson, K. N. *Can. J. Chem.* **2006**, *84*, 804−811.

(16) Otwinowski, Z. and Minor, W. In *Methods Enzymol*. Vol. 276. *Macromol. Crystallogr., Part A*. Academic Press: New York, 1997; pp. 307−326.

(17) *CrystalClear*: Rigaku Corp., 1999. CrystalClear Software User's Guide, Molecular Structure Corp., 2000. Pflugrath, J. W. *Acta Crystallogr*. **1999**, *D55*, 1718−1725.

(18) Blessing, R. H. *Crystallogr. Rev*. **1987**, *1*, 3−58.

(19) Farrugia, L. J. WinGX (Version 1.64.05). *J. Appl. Crystallogr.* **1999**, *32*, 837−838.

(20) *CrystalStructure 3.6.0*: Crystal Structure Analysis Package, Rigaku and Rigaku/MSC (2000−2004). 9009 New Trails Dr., The Woodlands, TX 77381.

(21) Farrugia, L. J. ORTEP-3. *J. Appl. Crystallogr*. **1997**, *30*, 565.

(22) Coppens, P. *X-ray Charge Densities and Chemical Bonding*; Oxford University Press Inc.; Oxford, U.K., 1997.

(23) Koritsanszky, T. S.; Howard, S.; Macchi, P.; Gatti, C.; Farrugia, L. J.; Mallinson, P. R.; Volkov, A.; Su, Z.; Richter, T.; Hansen, N. K. XD (version 4.10, July 2003), Free University of Berlin, Germany; University of Wales, Cardiff, U.K.; Universita di Milano, U.K.; CNR-ISTM, Milano, U.K.; University of Glasgow, U.K.; State University of New York, Buffalo, NY; University of Nancy, France, 2003.

(24) Munshi, P.; Row, T. N. G. *J. Phys. Chem. A* **2005**, *109*, 659−672.

(25) Clementi, E.; Raimondi, D. L. *J. Chem. Phys.* **1963**, *38*, 2686−2689.

(26) Allen, F. H. *Acta Crystallogr* **1986**, *B42*, 512−522.

(27) Semmingsen, J. *J. Chem. Phys.* **1977**, *66*, 4405.

(28) Robertson, K. N.; Knop, O.; Cameron, T. S. *Can. J. Chem.* **2003**, *81*, 727−743.

(29) Koch, U.; Popelier, P. *J. Phys. Chem.* **199**, *99*, 9747.

(30) Bondi, A. *J. Phys. Chem.* **1964**, *68*, 441−451.

(31) Nyburg, S. C.; Faerman, C. H. *Acta Crystallogr*. **1985**, *B41*, 274−279.

(32) Mallinson, P. R.; Smith, G. T.; Wilson, C. C.; Grech, E.; Wozniak, K. *J. Am. Chem. Soc*. **2003**, *125*, 4259.